Journal of
Applied Remote Sensing

New method for ship detection in synthetic aperture radar imagery based on the human visual attention system

Mehdi Amoon
Ahmad Bozorgi
Gholam-ali Rezai-rad

SPIE

New method for ship detection in synthetic aperture radar imagery based on the human visual attention system

Mehdi Amoon, Ahmad Bozorgi, and Gholam-ali Rezai-rad
Iran University of Science and Technology, Department of Electrical Engineering, Tehran, Iran
m_amoon@iust.ac.ir

Abstract. We propose a new algorithm for ship detection in synthetic aperture radar (SAR) images based on the human visual attention system. The human visual attention system identifies the prominent objects in images or scenes so that these objects can be more noticeable. Since the ships in a SAR image of the ocean are prominent objects, they can easily be identified through the human visual attention system. Thus, for detection of ships in the SAR images, the present study (through its application) has modeled the human visual attention system in the detection stage. In this way, not only can the targets be precisely detected, but also the falsely detected pixels are significantly reduced. Compared to most existing algorithms in the literature, our proposed algorithm can be used for both homogeneous and nonhomogeneous images. Accordingly, its performance is independent of the image type (homogeneous or nonhomogeneous) and the computation time significantly decreases. Experimental results have shown the efficiency of the proposed algorithm for various SAR images from ERS-1, ERS-2, and ALOS PALSAR data.
 [DOI: 10.1117/1.JRS.7.071599]

Keywords: ship detection; synthetic aperture radar image; relief map; human visual attention system.

Paper 12066V received Apr. 8, 2012; revised manuscript received Dec. 27, 2012; accepted for publication Jan. 28, 2013; published online Feb. 19, 2013.

1 Introduction

One of the most common active sensors for imaging operation is synthetic aperture radar (SAR). In recent years, high-resolution SAR images are widely used both in military and civilian applications. Much effort has been devoted to ship detection using SAR images. Because SAR images are less influenced by the time and weather conditions than the optical images, they are more suitable for ship detection.[1–10] Systems using this technique can efficiently perform the monitoring and surveillance mission of the sea surface. Ship detection is of great usefulness for maritime surveillance, fishery activity management, monitoring ship traffic, and, in particular, increasing maritime security by monitoring illegally operating ships, such as those involved in piracy activities.

There are two fundamentally different means of detecting ships in SAR imagery: detection of the ship target itself and detection of the ship wake. We note that most current research on ship detection is based on detecting the ship rather than its wake. First of all, the reflected signal from the ship as a feature is more useful and less dependent on the sea state and higher than the surrounding sea clutter. Moreover, the ship wakes are often invisible for some special angles of radar and, the detection of ship wakes needs heavy computational processing. Consequently, in this paper, we focus on the schemes of detecting ship targets themselves rather than ship wakes since ships have more robust backscattering properties than ship wakes, and ship wakes do not exist sometimes.[1]

Due to the corner reflection from the ship structure or between the ship body and ocean surface, ship targets are usually clear in SAR images. When the ocean surface is relatively calm (e.g., when the wind speed is lower than two meters per second), the reflection of the

ocean surface to the radar wave is specular reflection and the echo signal is very faint. In most research, the background of the SAR images is quite dark and targets are bright, so it is very easy to detect these ship targets. On the other hand, when the wind is fierce, large waves will be stirred. The backscattering echo will be very strong and the whole SAR image will be rather bright. This causes many difficulties in the detection of the ships, and especially small ships.[2,3]

The conventional method of ship detection uses constant false alarm rate (CFAR) in which the threshold value automatically adapts to the statistical distribution of the signal in a detection window.[2,3] The main disadvantage of CFAR is that if the signature of a ship has a similar intensity level as its surroundings, the extraction of ships becomes very difficult and has false alarms unavoidably. Other cross-correlation algorithms such as in Ref. 4, techniques based on wavelet,[5,6] detection methods based on polarization[7,8] and Lognormal distributions,[9] Weibull,[10] K,[11–13] and α-stable[14,15] have also been suggested. When using these distributions for modeling the sea clutter in a CFAR algorithm, we find that they either produce a lot of false alarms or miss some ship target detections. However, none of them can be the same with all the clutter backgrounds in SAR images. For the homogeneous areas of the SAR clutter background, Gauss, K, and G^0 distribution can be used to model the clutter. Compared with other distributions, Gauss distribution has many advantages, such as fewer undetermined parameters, less calculation complexity, and easy realization. For the heterogeneous areas of the SAR clutter background, only K and G^0 distribution can have a good effect to simulate the SAR clutter background. However, parameter estimation needs complex numerical calculations and takes a lot of time.[11–13] Therefore, the algorithms utilized in this distribution are far less effective in real-time detection systems and cannot detect a target whose intensity is at a similar level to the clutter. Articles employing K distribution have used processing of the small size images with low resolution in order to decrease processing time.

Most research studies on ship detection in SAR images have chosen homogeneous and uniform images of ocean surface.[16–18] Homogeneous images of the ocean surface does not contain harbor areas, urban areas, and oil spills. However, some studies have recently been conducted in order to deal with nonhomogeneous SAR images consisting of nonuniform ocean surface. Nonuniform ocean surface is usually the result of oil spills, wind, or some other geographical factors.[19–23] Nevertheless, nonuniformities of these images are not as much as the nonuniformities of the nonhomogeneous images, including harbor areas, urban areas, and mountains.[24–26]

All the algorithms used for ship detection in the homogeneous SAR images are to reduce the noise from the sea and detect the ships without any visible falsely detected pixels. In addition to the noise reduction for ship detection in nonhomogeneous SAR images, it is also required to remove the areas of images with intensity the same as or more than the ship area's intensity.[25] Furthermore, the background of homogeneous SAR images is exactly the ocean surface, while the background of nonhomogeneous SAR images is usually composed of several different scenes. Thus, unlike the homogeneous images that require only a simple distribution for modeling clutter of background (such as Gaussian distribution), nonhomogeneous images need a relatively complex distribution.

It should be noted that most papers have presented algorithms for either homogeneous or nonhomogeneous images, while there are only a few papers considering both homogeneous and nonhomogeneous images.[22] There are two main difficulties in making recommendations. First, different types of imagery require different algorithms. Second, there is a lack of rigorous performance evaluation in the literature. Often the imagery is visually ground-truthed and some algorithms are very poorly tested with results only being presented for a small number of images. This makes comparison of the various approaches difficult.

In this paper, we have presented a new algorithm for ship detection in SAR images based on the human visual attention system. In contrast with most existing algorithms in the literature, our proposed algorithm can be used for both homogeneous and nonhomogeneous images. While dealing with nonhomogeneous images, this algorithm has a quite acceptable processing time and its computational efforts are also reasonable. Furthermore, in order to evaluate the efficiency and reliability of the proposed approach, various SAR images have been applied. The rest of this paper is organized as follows. Section 2 introduces the paper methodology. Experimental results are provided in Sec. 3. Finally, concluding remarks are provided in Sec. 4.

2 Methodology

Figure 1 represents the flowchart of the suggested approach. Our proposed algorithm falls into two main stages; concerning the function of each step, the first stage is here called the preprocessing stage and the second one is named as the detection stage. There will be the same preprocessing stages on both right-hand and left-hand paths of the flowchart in Fig. 1.

In the first stage, the land areas of the image such as cities, harbors, mountains, etc. are removed as much as possible. Simultaneously, the noise of the sea surface is significantly reduced. The input SAR images have been divided into 75×75 pixel subimages in the left-hand path, as shown in Fig. 1. Then, independent processing of each subimage is performed based on step 2, and finally the minimum of both right-hand and left-hand paths is calculated. Now the input SAR images are preprocessed and ready to be used in the detection section. By the second stage, the T_F threshold is applied to the final preprocessing image; the desired object inspired by the human visual attention system is detected; and finally pulse cosine transform (PCT) is employed.

2.1 *Preprocessing Stage: Removing Land Areas and Reducing Noise at Sea Surface*

In this stage, a new algorithm for removing high-intensity land areas from the SAR image has been proposed. Simultaneously, the noise of the sea surface is considerably reduced. In the following, different steps in the preprocessing stage are described.

Step 1: Input image is partitioned into several square subimages of equal sizes (Fig. 2).

The size of the subimages depend on various parameters, including image resolution, size of the smallest and largest ship in the image, noise of the sea surface, minimum distance between the ships, and minimum distance between ships and land areas in the image. In this paper, a subimage size equal to 75×75 pixels has empirically been considered.

Step 2: Processing of each subimage is performed as follows:

A moving window of 3×3 pixels is applied to each subimage (Fig. 2). This moving window is shifted one pixel sequentially until the entire subimage pixels are swept. In each shift, the value of ν is calculated from Eq. (1) and its value is substituted into the central pixel of the moving window.

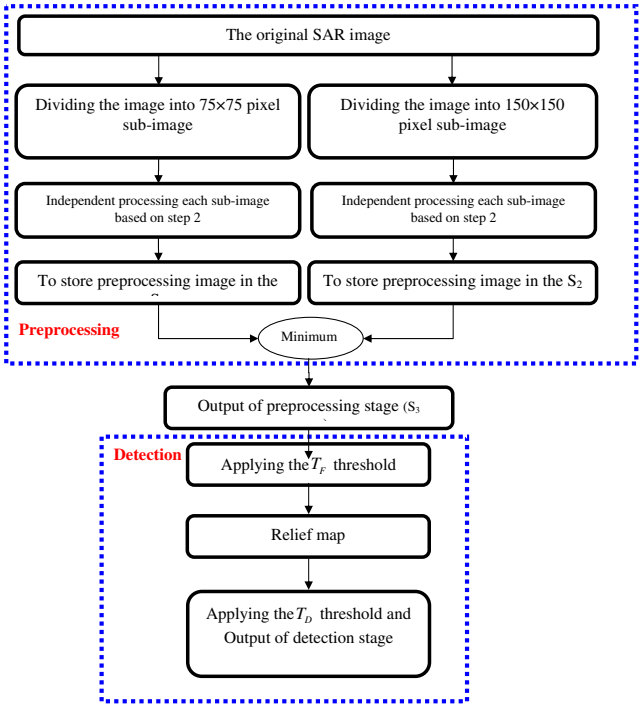

Fig. 1 Block diagram of the proposed algorithm.

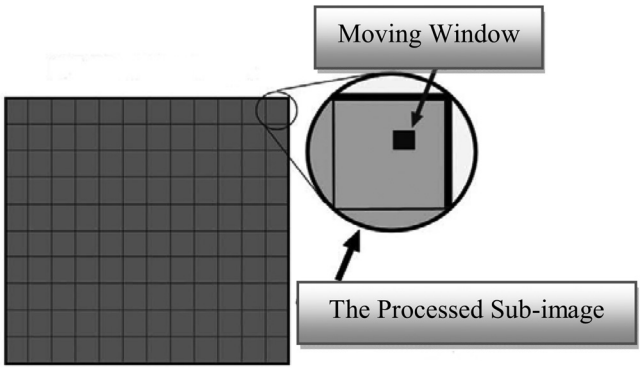

Fig. 2 Dividing of the image into the square frames with the same size and processing of each subimage.

$$\nu = \frac{[\mu_{\text{local window}}]^2}{2[\sigma_{\text{tile}}]^2}, \tag{1}$$

where $\mu_{\text{local window}}$ is the average of pixels in the moving window, and σ_{tile} is standard deviation of all pixels in the processed subimage. ν indicates the group of pixels which is brighter than other pixels in the subimage.[27]

This operation removes land areas and many pixels with high brightness but maintains the ships with only a few pixels. As an illustrative example, consider a subimage t_1 in which there are one or more ships, and the remaining pixels create the background. Consider another subimage t_2 where all or most of its pixels have formed the dry area in the image. Due to the fact that combination of dry area (inland area) with sea area provides nonuniform SAR image significantly, data scattering over the t_2 subimage is much higher than the data scattering in t_1.

Consequently, the standard deviation (SD) of pixel values in the t_2 subimage is much greater than that of t_1. On the other hand, the standard deviation square of each subimage is in the denominator of Eq. (1); as a result, for the nonuniform subimage t_2 with great SD, the value of ν becomes very small. In contrast, for the t_1 subimage consisting of the ship or part of it, SD is rather small. This leads to a greater value for ν which in turn causes the ships to be seen more clearly.

Step 3: In this step we assume that step 2 of the processing operation has been performed for all subimages.

Note that the boundary of the ocean regions and other areas (e.g., urban areas, port areas, mountains, etc.) is usually bright and has high intensity. Consider a subimage in which most pixels are associated with the ocean and just a few pixels are related to the border areas with higher values of intensity. This subimage is similar to a subimage consisting of a ship with a few bright pixels and ocean background with darker pixels.

After step 1 of the processing operation, the edges of the processed image become brighter than the surrounding environment. This can clearly be observed in Fig. 3(b).

The result of applying the proposed algorithm in step 1 to the SAR image is presented in Fig. 3(a) where 19 fishing boats on the sea surface are the desired objects for detection.

In order to avoid this undesired situation, we add an extra processing step to ensure that none of the subimages in the image undergoes conditions such as those mentioned in the previous example. For this purpose, the result of step 2, a preprocessing image such as Fig. 3(b), is stored as the S1 image. Then, the size of subimages is slightly altered and steps 1 and 2 are repeated again with the new subimage sizes, like 150×150 pixels. Finally, the result is stored again and we call it the S_2 image. The result of repetition of step 2 of the processing with the new subimage size is that subimages with ocean area as a major part and with only a few bright boundary pixels dramatically change. Two types of change can be distinguished for them: either bright boundary pixels have gone outside the new subimages or brighter boundary pixels have come into the new subimages. In both cases, the bright borders in the new subimages are not

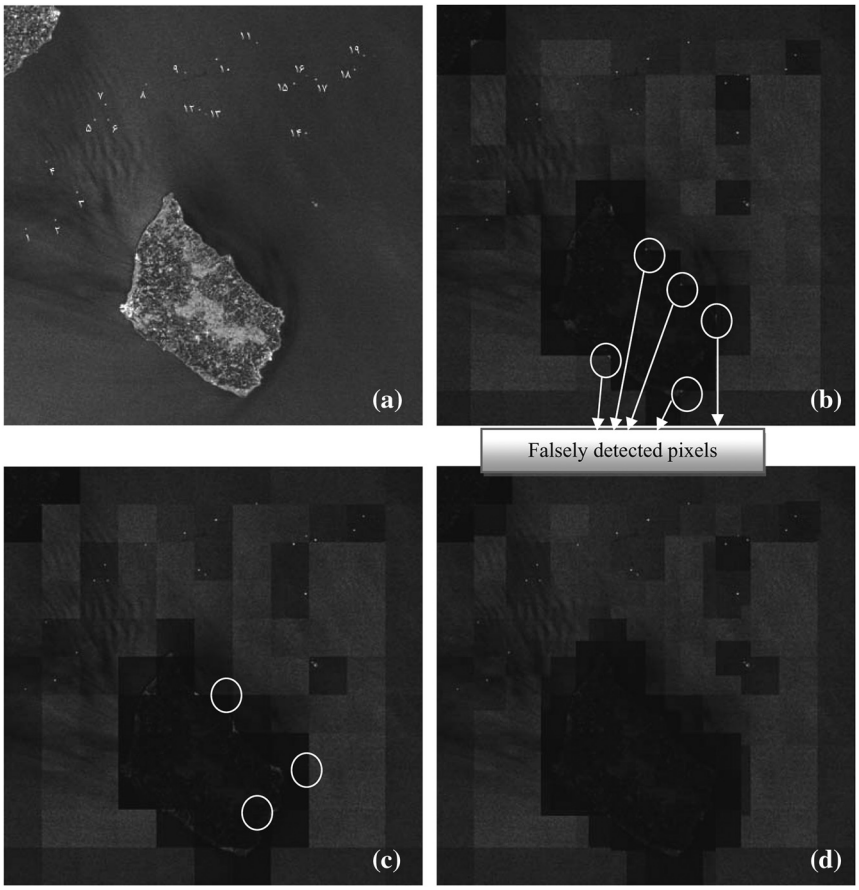

Fig. 3 (a) The original image. (b) The preprocessing image with a subimage size equal to 75×75 pixels. (c) The preprocessed image with a subimage size equal to 150×150 pixels. (d) Output of the preprocessed stage.

detected as the desired objects by our algorithms (note that in the second case, where brighter boundary pixels come into the subimage, the standard deviation of the subimage becomes greater and then ν significantly decreases). Of course in the new S_2 image, new subimages with undesired conditions may also be produced (although we have just tried to avoid them). This can be a dilemma for our method; fortunately this problem can be solved by a simple trick. In the images S_1 and S_2, peer to peer subimages do not have similar conditions; therefore, bright boundary pixels are not common for the corresponding subimages in the images while the ship in both images is clearer than their surrounding environment. So a new image, S_3, of which each pixel is a minimum of corresponding pixels in S1 and S_2 is obtained. Therefore, S_3 is an image, of which the bright pixels are only the ship pixels, and so the ship in the image can be detected without any undesired boundary pixels.

Figure 3(c), displays the result of steps 1 and 2 with the 150×150 size of subimage, and Fig. 3(d) displays the minimum of Fig. 3(b) and 3(c).

As mentioned before, the subimage size depends on several parameters. One of these parameters is image resolution. The subimage size directly depends on the image resolution; for higher resolution images, the bigger subimage size should be selected. Bigger subimage size in turn increases the standard deviation of subimages. Although a greater standard deviation reduces the noise of the image, it may deteriorate the ship detection process. If the subimage size is inappropriately selected, it may lead to the removal of one or more ships in the preprocessed image. The combination (75×75, 100×100), (95×95, 100×100) and (100×100, 150×150) subimage size can be considered as good options for our SAR images.

However, our experimental results have shown that the combination (75×75, 150×150) yields the best results for our SAR images.

2.2 *Detection Stage*

Visual attention is one of the most important parts of consciousness.[28,29] In fact, most of the information that a person receives from the outside is through the visual system. It has been proved that the human visual attention system has a mechanism to stare at prominent objects in a scene or landscape.[28] When we look at a scene or image, there are some prominent and noticeable objects which attract much of our attention. In this context, the human visual attention system, similar to a spotlight, quickly sweeps the entire visual field and selects the prominent objects. Then, our visual attention system sends their images to our short-term memory and causes us to gaze at them.

Along with neurological studies on the human visual attention system, some artificial intelligence researchers have sought to find a complete computational model for the visual attention system. Recently, several papers studying the computational model for the visual attention system have been published. In Ref. 30, an acceptable biological model for the human visual attention has been introduced, of which the attention mechanism has been developed in Ref. 31. Some new approaches based on Fourier transform (FT) have been proposed in Refs. 31–33. These approaches can accurately highlight the prominent areas of an image in a minimum time. Finally, Refs. 34 and 35 have proposed new transforms called pulsed principal component analysis (P2CA) and pulsed cosine transform (PCT) to enhance and complete the previous models. Figure 4 shows an example of the PCT model for computing the relief map of a natural landscape. A relief map shows the different heights of the land forms using color shading and lines. The bright areas in the relief map attract human visual attention more than the dark areas.

It has been mentioned that the human eye is superior to existing automatic algorithms in observing a slick in the context of the surrounding sea, and surprisingly, some vessels undetected by conventional techniques are visible to the eye.[5,36] Inspired by this rationale, a simple and effective algorithm is proposed based on the application of the human visual attention model for ship detection. In this paper, PCT is selected for visual attention model due to its computational efficiency and its great capability to predict eye fixation. Further details on the subject are provided in Ref. 34. Steps in the algorithm are as follows.

Step 1: In this step, a thresholding process is used to remove noisy pixels and enhance the binary image quality for the next step. For this purpose, the final preprocessed image of the previous stage (S_3) is used for computing the threshold value. The threshold value is calculated from the following equation:

$$T_F = \mu_{S3} + (\alpha \times \sigma_{S3}), \tag{2}$$

where μ_{S3} and σ_{S3} are the mean and standard deviation of S_3, respectively, and α is a constant value. A greater value of α increases the value of the threshold and decreases the noise of the image. On the other hand, an inappropriate large value of α causes some pixels of the ship to be segmented as noisy pixels, so the value of α should be carefully chosen. In this paper, we set $\alpha = 0.6$. The thresholding process is performed through the following equation:

$$S_4(x,y) = \begin{cases} S_3(x,y), & \text{when} \quad S_3(x,y) \geq T_F \\ T_F, & \text{when} \quad S_3(x,y) < T_F \end{cases}. \tag{3}$$

Now, the enhanced binary image S_4 is ready for the visual attention model input.

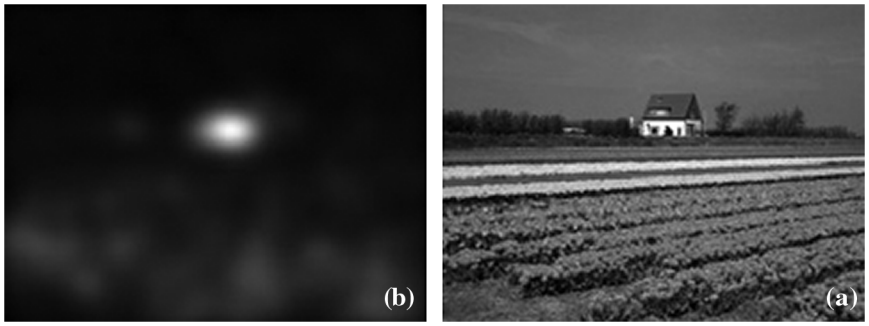

Fig. 4 (a) The original image. (b) Relief map.

Step 2: In this step, a new PCT-based model for visual attention is introduced. This model produces relief map of the input image. With S_4 as an input image, the human visual model will be illustrated in the following

$$P = \text{sign}[c(S_4)] \tag{4}$$

$$F = c^{-1}(P), \tag{5}$$

where c and c^{-1} are two-dimensional discrete cosine transform (DCT) and its inverse, respectively.[37] Mark sign$(\cdot)$ is sign function. Note that F is non-negative and negative values of inverse DCT are set to zero. Then, a Gaussian filter is used for smoothing the result

$$S_{\text{saliency}} = G * F^2, \tag{6}$$

where G is a two-dimensional low-pass Gaussian filter and the "*" symbol is the convolution operator. Note that F is squared in Eq. (6) for visibility.

Equation (4), which is adopted from Ref. 34, is called the pulsed cosine transform (PCT). This equation holds only the sign of DCT coefficients and the amplitude of DCT coefficients is not used. A detailed description of this model has been provided in Refs. 34 and 35.

Step 3: In this step we complete our ship detection algorithm by an adaptive thresholding process. Although in this step, ship detection can be performed using a fixed threshold, a constant threshold is not applicable for all cases. An adaptive threshold determined by the image values is used for efficient object detection. The adaptive threshold for automatic detection of ships is obtained through the following equation:

$$T_D = \mu_{Ss} + (\beta \times \sigma_{Ss}), \tag{7}$$

where μ_{Ss} and σ_{Ss} are the mean and standard deviation of the relief map, respectively. β is a constant which is empirically adjusted. Finally, ship detection is done using the following equation:

$$D(x,y) = \begin{cases} 1, & \text{when} \quad S_{\text{saliency}}(x,y) \geq T_D \\ 0, & \text{when} \quad S_{\text{saliency}}(x,y) < T_D \end{cases}. \tag{8}$$

Usually, the deviation of the relief maps with ship signatures is small, while the deviation of the relief maps without any ship signature is comparatively large. Therefore, given a proper parameter β and calculated by Eq. (8), the detection threshold for a ship-free relief map can become large enough to avoid false alarms. In this paper, we choose $\beta = 14.5$ empirically based on the observations and experimental results.

Figure 5(a) is the result of applying the threshold to the image in Fig. 3(d). Figure 5(b) is the relief map of Fig. 5(a) and 5(c) shows the final detected image. Our algorithm result has only one falsely detected pixel [Fig. 5(c)] of which the size and shape are very similar to those of the desired targets.

As mentioned before, dimensions of the subimage depend on the minimum distance between ships and land areas in the image. If the distance of a ship is smaller than the size of the subimages, the ship is not detected. For example, if the size of subimage is 75×75 pixels, then the minimum distance between the ships and the coastal area can be 75×75 pixels. Simulation results for the subimage sizes (150×150, 550×550), which have been used concomitantly, are shown in Fig. 6. As it can be seen, the targets on the left half of the image have not been detected through the subimage size equaled to 550×550 pixels [Fig. 6(c)] while all targets have been detected through the subimages size equaled to 150×150 pixels [Fig. 6(b)].

3 Experimental Results

In this section, the experimental results of the proposed algorithm are shown. To ensure the accuracy and efficiency of the algorithm for ship detection, a wide variety of homogeneous and nonhomogeneous SAR images are used. In all test images, the subimage size of

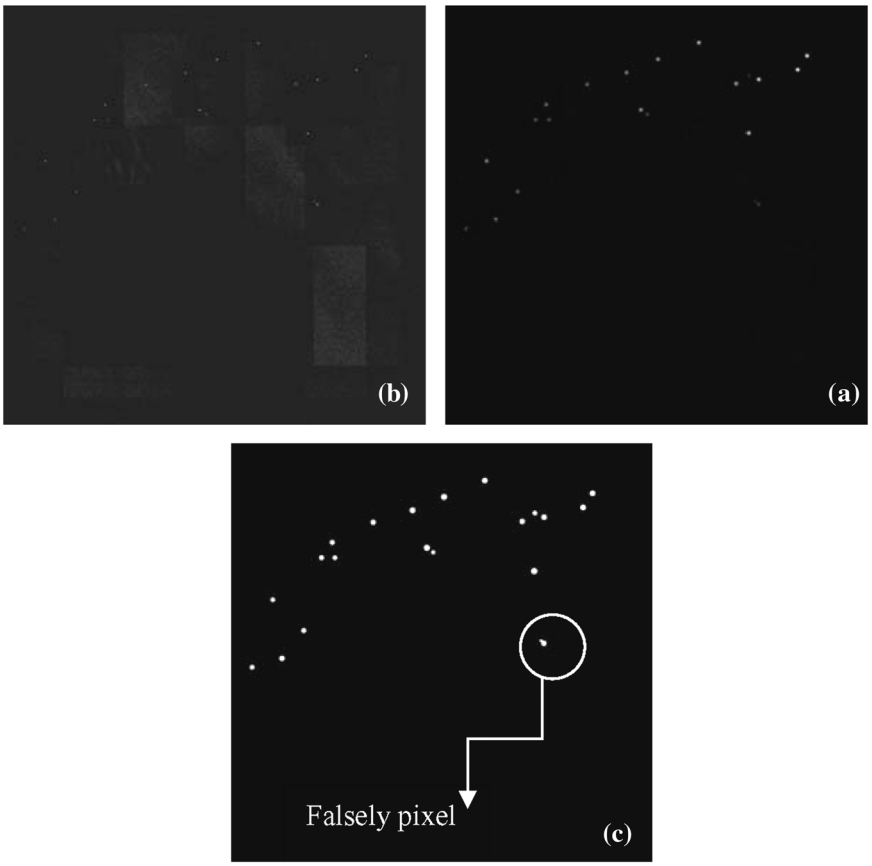

Fig. 5 (a) Enhanced image of the first step of the detection stage. (b) Relief map. (c) Output of the detection stage.

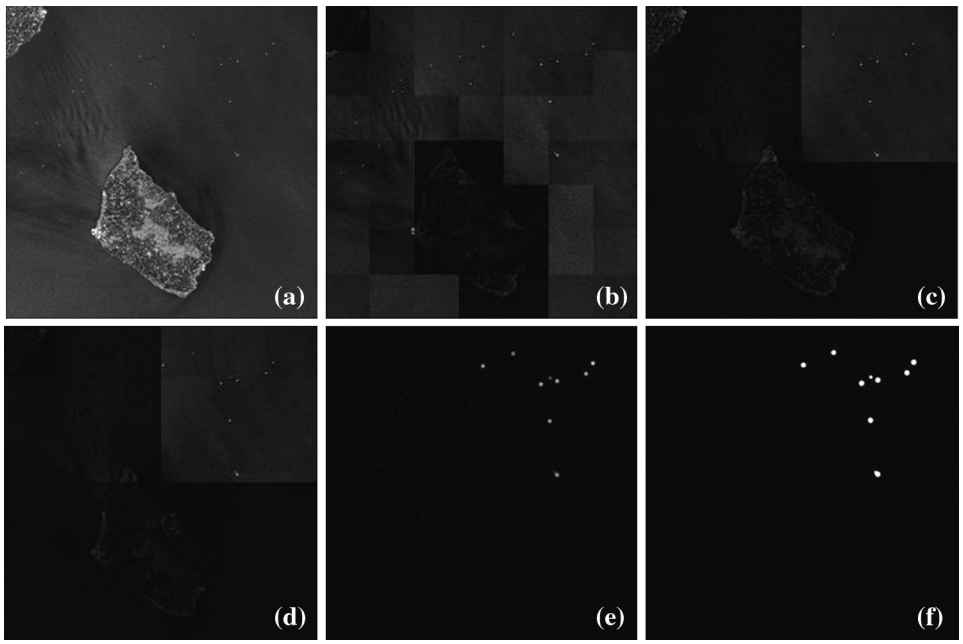

Fig. 6 (a) The original image. (b) The preprocessing image with a subimage size equal to 150×150 pixels. (c) The preprocessed image with a subimage size equal to 550×550 pixels. (d) The enhanced image of the first step of the detection stage. (e) The relief map of the final preprocessed image. (f) The output of the detection stage.

$(150 \times 150, 75 \times 75)$ for the preprocessing stage is used and for the detection stage we choose $\alpha = 0.6$ and $\beta = 14.5$. Also, for each SAR image the results of the preprocessing (S_3 image) and detection stage (resulted relief maps and final detected image) are shown. In addition, the results of the proposed algorithm are compared with a conventional CFAR detector with a 0.5% false pixel detection rate.

It should be noted that some previous research has defined a significance parameter for measuring the ability of the algorithm for target clarity (such as Refs. 5 and 36). In this paper, the significance parameter is used to measure the ability of the relief map of the proposed algorithm for clarifying of the targets. Like previous works in the literature, significance is defined as follows:

$$\text{significance} = \frac{\theta_T - \mu_B}{\sigma_B}, \tag{9}$$

where μ_B and σ_B are the mean and standard deviation of the background, respectively, and θ_T is the maximum of the target values.

Example 1: Figure 7(a) shows a SAR image (280×280 pixels) in which a ship is represented. Detection of the ship in this image is somewhat difficult, because the speckle is very strong. Figure 7(b) to 7(e) displays the CFAR detection, the preprocessing stage, relief map, and the detection result of out method, respectively. As can be observed, the ship detection is completely successful without any falsely detected pixels. The conventional CFAR method would cause false alarms even though it works at a very low false alarm rate.

Example 2: Figure 8(a) shows a SAR image (1160×770 pixels) taken by ERS-2 which belongs to the area size of 14.5×9.7 km^2. In the top right corner of the image there is a

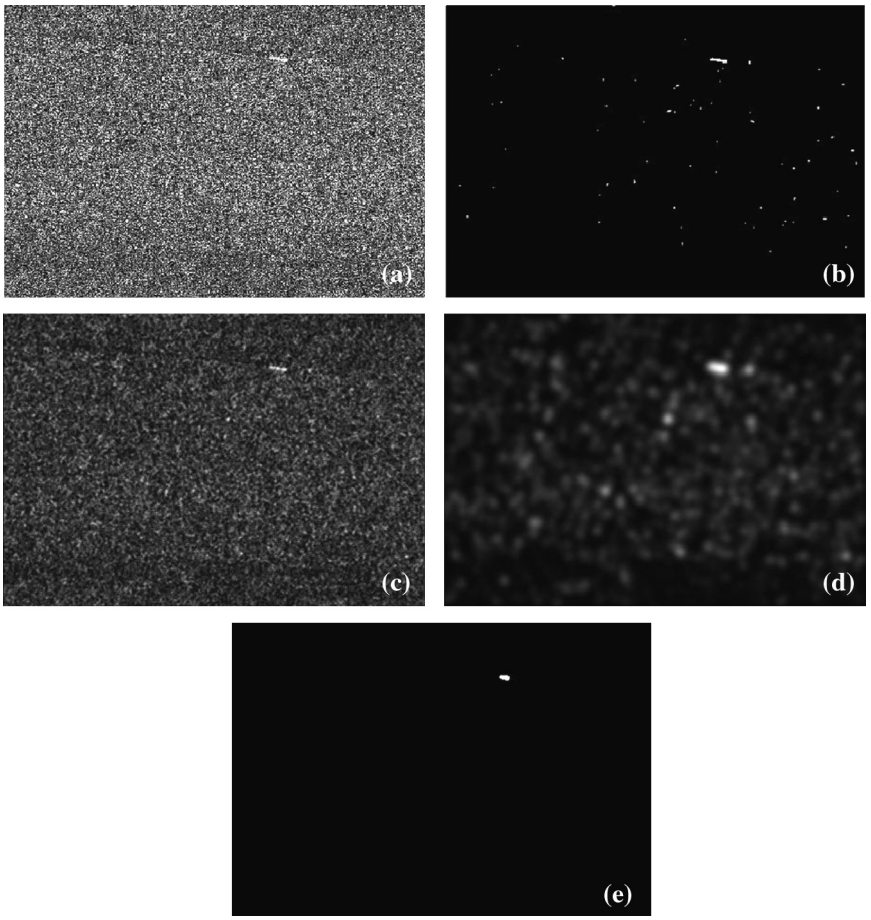

Fig. 7 (a) ALOS SAR image (significance = 2.38). (b) Detection result of CFAR. (c) The final preprocessed image (significance = 7.68). (d) The relief map of the final preprocessed image (significance = 17.70). (e) Output of the detection stage.

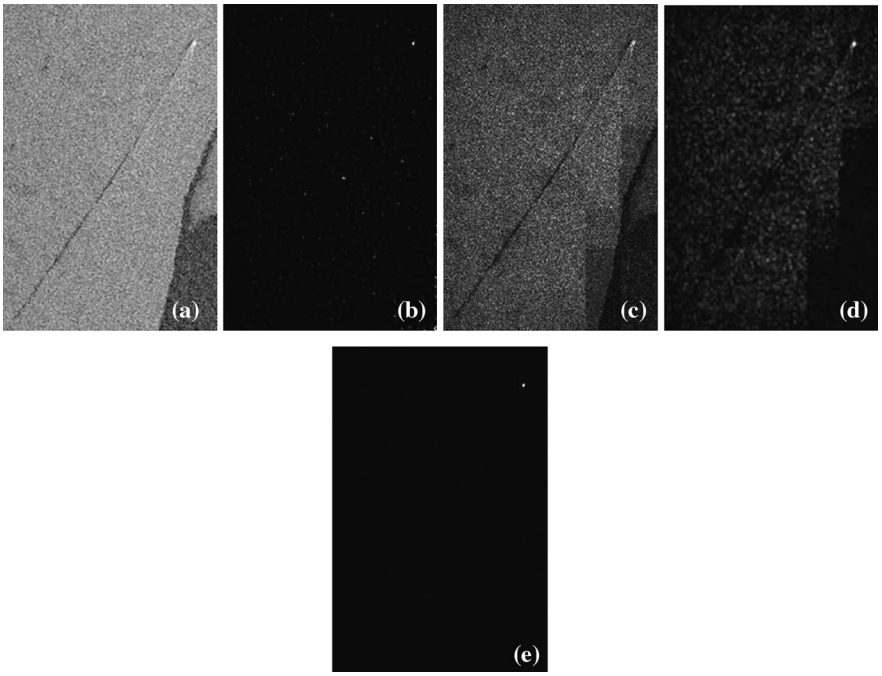

Fig. 8 (a) SARERS-2 image (significance = 3.07). (b) Detection result of CFAR. (c) The final preprocessed image (significance = 5.34). (d) The relief map of the final preprocessed image (significance = 24.68). (e) Output of the detection stage.

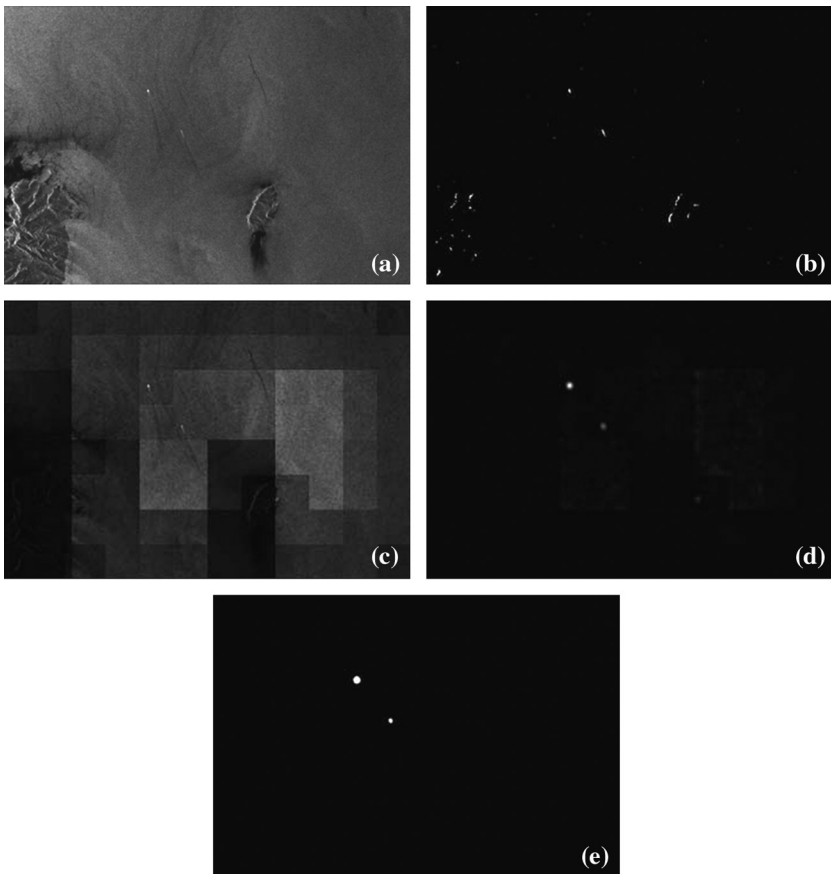

Fig. 9 (a) SARERS-2 image (significance = 8.34). (b) Detection result of CFAR. (c) The final preprocessed image (significance = 11.88). (d) The relief map of the final preprocessed image (significance = 84.85). (e) Output of the detection stage.

ship with a long wake. Also in the bottom right corner, there is a dark area. The darkness of this area is due to sea turbulence which has caused a weak signal has been reflected towards the radar. Due to the dark area in the image, it is a nonuniform image, which aggravates the ship detection process. However, our algorithm appropriately detects the ship without any falsely detected pixels.

Example 3: Figure 9(a) shows an image of ERS-2 SAR (840×580 pixels) from Corsica Island in the Mediterranean Sea. Land areas and black spots in the image have made a very heterogeneous region. In this image, there are two ships that our algorithm detects them completely without any falsely detected pixels.

Example 4: Figure 10(a) shows an image of ERS-2 SAR (570×870 pixels) in which there is a ship. Bottom left corner shows the small city of Bastia. This city and its bright spots have made this SAR image very heterogeneous. But as it is observed, our algorithm completely detects the ship without falsely detected pixels.

Example 5: Figure 11(a) shows an image of ERS-1 SAR (437×473 pixels) from Genova in Italy in which there are two tanker ships in the front harbor. This is a very noisy and heterogeneous image. But as it is observed, the ships have been completely detected by our algorithm without any falsely detected pixels.

Example 6: In order to test the reliability of the proposed algorithm, two SAR images without any ships have been used in this example. Figure 12(a) shows the two SAR images (256×256 pixels) without any ship signature. The first image is homogeneous regions and the second one is heterogeneous regions. Our algorithm in both images neither detects any target, nor has any falsely detected pixels. Thus, there is no false detection in the output of our method. Note that CFAR still has false alarms in this case.

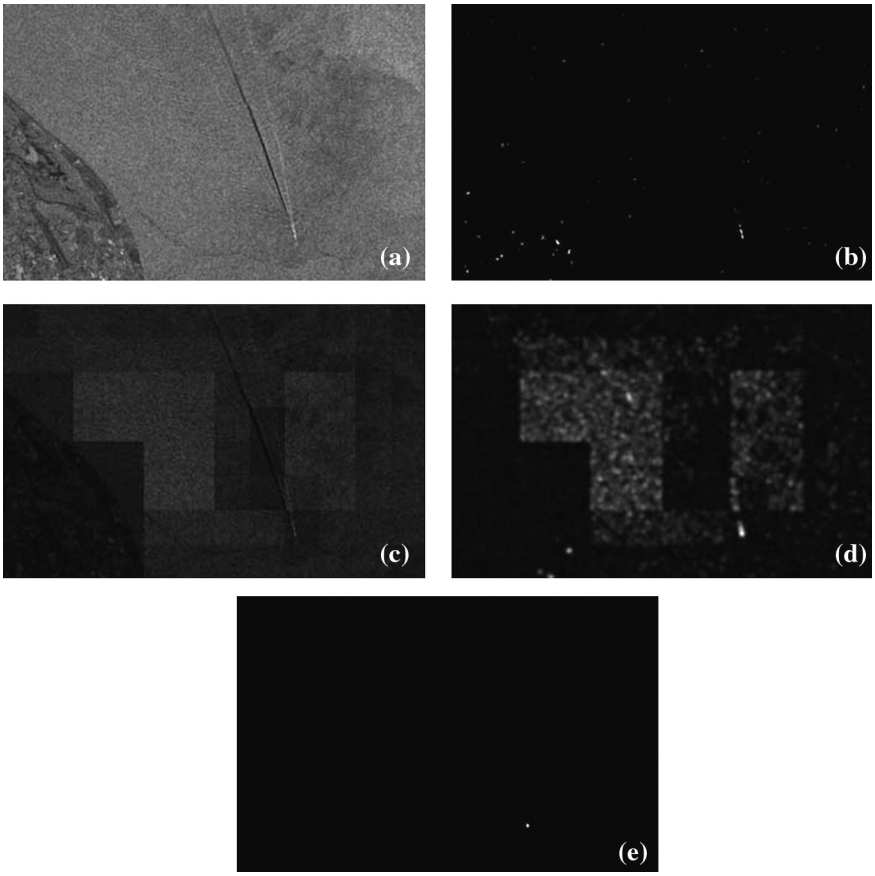

Fig. 10 (a) SARERS-2 image (significance = 4.98). (b) Detection result of CFAR. (c) The final preprocessed image (significance = 6.18). (d) The relief map of the final preprocessed image (significance = 17.89). (e) Output of the detection stage.

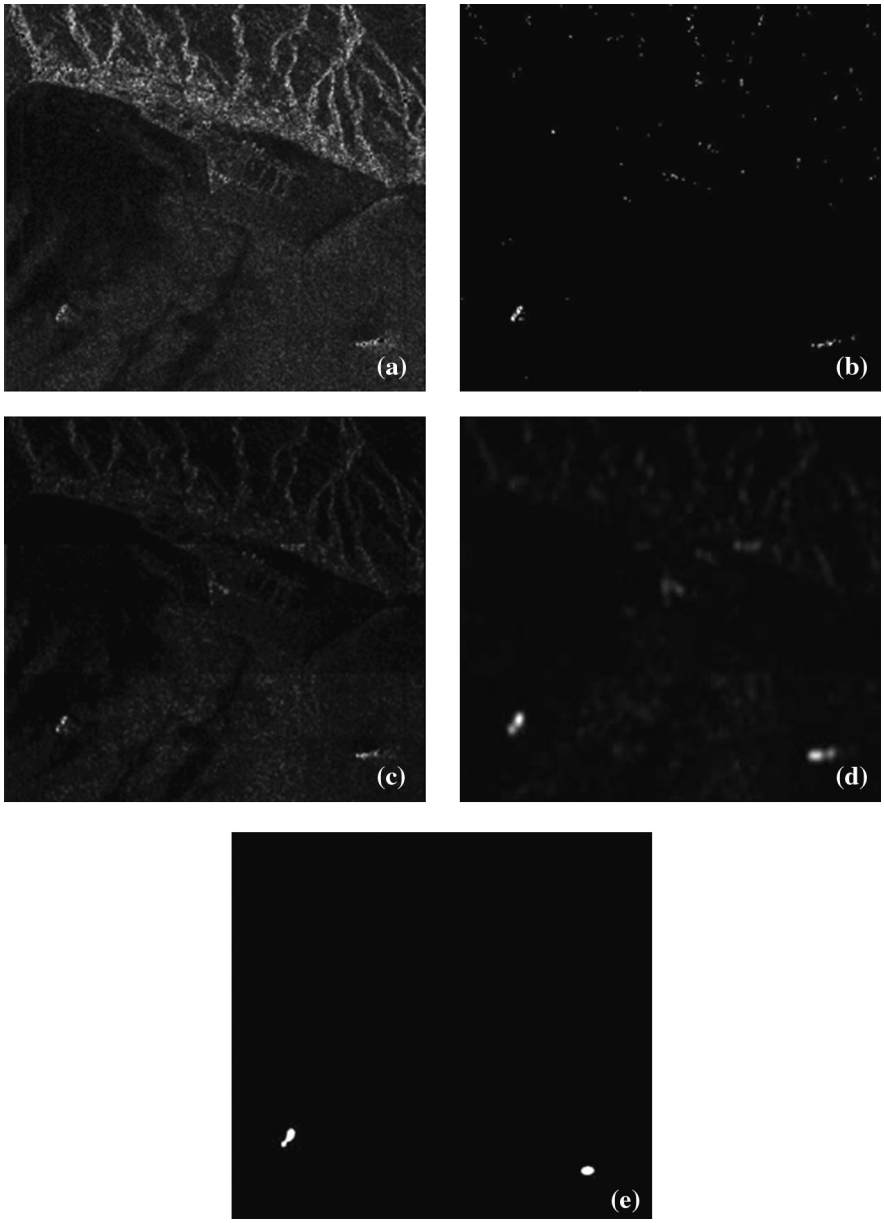

Fig. 11 (a) SARERS-1 image (significance = 7.17). (b) Detection result of CFAR. (c) The final preprocessed image (significance = 24.17). (d) The relief map of the final preprocessed image (significance = 34.36). (e) Output of the detection stage.

The ground truths of SAR images are located at the following addresses in Refs. 38 and 39.

The experiments were conducted using a PC with Pentium Dual-Core CPU of 2.8 GHz and memory of 4 GB. The program codes were written in MATLAB. For the image shown in Fig. 8, the computation times of the proposed detector and the two detectors used for comparison are displayed in Table 1.

It is noticed that the proposed detector consumes less time than the CFAR-based Gaussian distribution and CFAR-based K distribution detectors since no distribution parameter estimation is required.[1,13]

In order to make further comparison between the CFAR algorithm and the proposed algorithm, we derive the receiver operating characteristic (ROC) curve. A plot of the target detecting probability (Pd) versus false alarm ratio (Pf) with changing the decision threshold is called receiver operating characteristic (ROC).[40]

The ROC curves corresponding to the CFAR and proposed detectors are shown in Fig. 13, where Pf and Pd are defined as[40]

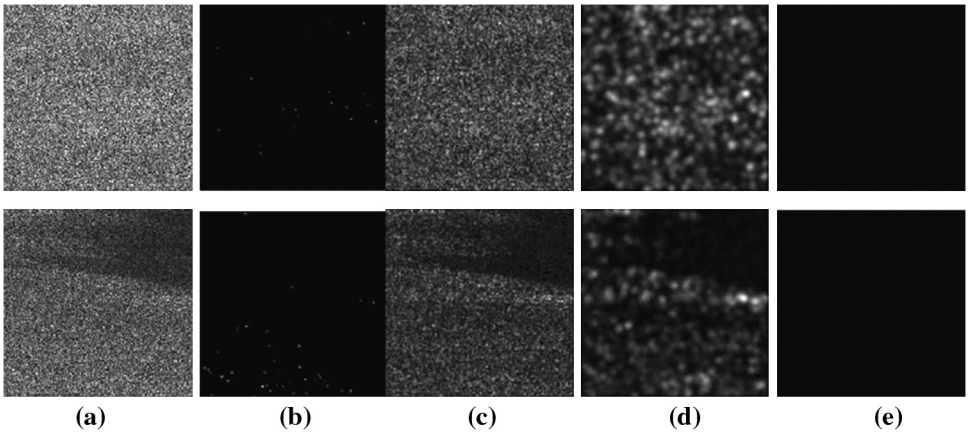

Fig. 12 (a) ALOS SAR image. (b) Detection result of CFAR. (c) The final preprocessed image. (d) The relief map of the final preprocessed image. (e) Output of the detection stage.

Table 1 Computation time of the proposed detector and the three detectors used for comparison, including the CFAR based on Gaussian distribution and CFAR based on K distribution detectors.

Detector	Proposed detector	CFAR based on Gaussian distribution	CFAR based on K distribution
Computation time (s)	0.68	3.54	11.2

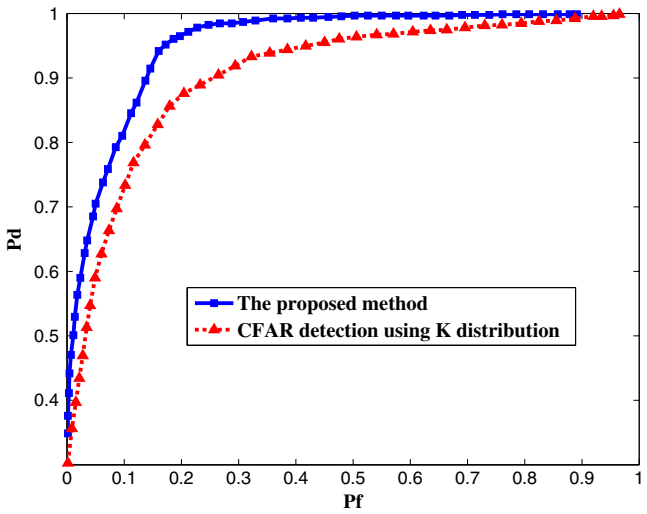

Fig. 13 Comparison of the ROC plot for detection performance.

$$\mathrm{Pf} = \frac{\text{Number of clutter chips detected as target chips}}{\text{Total number of clutter chips}}, \tag{10}$$

$$\mathrm{Pd} = \frac{\text{Number of target chips detected as target chips}}{\text{Total number of target chips}}. \tag{11}$$

As shown in Fig. 13, combining Eqs. (10) and (11), we obtain the receiver operating characteristic curves of the CFAR algorithm using K distribution and the presented method. These curves indicate that the method in this study has better detection precision than the CFAR algorithm based on K distribution.

4 Conclusion

In general, the CFAR detector or its enhanced variations are used for ship detection in the SAR images. The efficiency and performance of the CFAR detector are always influenced by the speed and accuracy. On the other hand, variations in these parameters in the CFAR detector are in opposite directions. That is, an increase in the speed results in a decrease in the accuracy and vice versa. Consequently, there has to be a trade-off between speed and accuracy in order to reach the optimum performance for these algorithms. Most of the algorithms proposed for ship detection in SAR images have sought to maintain the accuracy while boosting the speed.

However, these efforts have not always been successful and most of these algorithms have only yielded good results for special images, which are not efficient enough compared to the other types of images. In the present study, it has been sought to address this problem through the application of the human visual attention system for the detection of the desired objects.

To perform the ship detection in SAR images, a new algorithm based on the human visual attention system has been proposed. In the first stage, the preprocessed stage, the high-intensity land areas of the image are removed, and noise of the sea surface is considerably reduced. In the second stage, the detection stage, this study has, thus, modeled the human visual attention system in the detection stage. In this context, not only can the targets be precisely detected but also the falsely detected pixels are significantly reduced. Besides, processing speed significantly increases. Furthermore, it is appropriate for real-time applications.

The significance parameter has been used to measure the capability of the relief map of the proposed algorithm for clarification of the targets. The experimental results indicate that, with our proposed method, the significance parameter is improved more than 10 times compared to the CFAR algorithm. Several ERS-1, ERS-2, and ALOS PALSAR SAR images have been used to justify the proposed algorithm. Compared to a typical CFAR algorithm, our proposed algorithm shows better efficiency in detecting ships for both homogeneous and nonhomogeneous images. As the results show, false alarms in the candidate chips are greatly suppressed, while most real ship targets are well maintained.

References

1. D. J. Crisp, "The state-of-the-art in ship detection in synthetic aperture radar imagery," Defense Science and Technology Organization Research Report, DSTO-RR-0272 (2004).
2. F. Zhang and B. Wu, "A scheme for ship detection in inhomogeneous regions based on segmentation of SAR images," *Int. J. Rem. Sens.* **29**(19), 5733–5747 (2008), http://dx.doi.org/10.1080/01431160802089887.
3. M. Liao et al., "Using SAR images to detect ships from sea clutter," *IEEE Geosci. Rem. Sens. Lett.* **5**(2), 194–198 (2008), http://dx.doi.org/10.1109/LGRS.2008.915593.
4. K. Ouchi et al., "Ship detection based on coherence images derived from cross correlation of multilook SAR images," *IEEE Geosci. Rem. Sens. Lett.* **1**(3), 184–187 (2004), http://dx.doi.org/10.1109/LGRS.2004.827462.
5. M. Tello, C. Lopez-Martinez, and J. Mallorqui, "A novel algorithm form ship detection in SAR imagery based on the wavelet transform," *IEEE Geosci. Rem. Sens. Lett.* **2**(2), 201–205 (2005), http://dx.doi.org/10.1109/LGRS.2005.845033.
6. M. Tello et al., "Use of the multiresolution capability of wavelets for ship detection in SAR imagery," in *Proc. IEEE Int. Geosci. and Remote Sens. Symposium*, Vol. 6, pp. 4247–4250, IEEE, Anchorage, Alaska (2004).
7. R. Touzi, "Calibrated polarimetric SAR date for ship detection," in *Proc.IEEE Int. Geosci. and Remote Sens. Symposium*, Vol. 1, pp. 144–146, IEEE, Honolulu, Hawaii (2000).
8. R. Touzi, "On the use of polarimetic SAR date for ship detection," in *Proc. IEEE Int. Geosci. and Remote Sens. Symposium*, Vol. 2, pp. 812–814, IEEE, Hamburg, Germany (1999).
9. A. Farina, A. Russo, and F. A. Studer, "Coherent radar detection in log-normal clutter," *IEE Proc. F Commun. Radar Signal Process.* **133**(1), 39–53 (1986), http://dx.doi.org/10.1049/ip-f-1:19860009.

10. R. Rifkin, "Analysis of CFAR performance in Weibull clutter," *IEEE Trans. Aerosp. Electron. Syst.* **30**(2), 315–328 (1994), http://dx.doi.org/10.1109/7.272257.
11. M. T. Rey, A. Drosopoulos, and D. Petroyic, "A search procedure for ships in radarsat imagery," Defense Research Establishment, Ottawa, Canada (1996).
12. H. C. Chan, "Radar sea clutter at low grazing angles," *IEE Proc. Radar Signal Process.* **137**(2), 102–112 (1990), http://dx.doi.org/10.1049/ip-f-2.1990.0015.
13. S. Erfanian and V. T. Vakili, "Introducing excision switching-CFAR in K distributed sea clutter," *Signal Process.* **89**(6), 1023–1031 (2009), http://dx.doi.org/10.1016/j.sigpro.2008.12.001.
14. C. Wang, M. Liao, and X. Li, "Ship detection in SAR image based on the alpha-stable distribution," *Sensors* **8**(8), 4948–4960 (2008), http://dx.doi.org/10.3390/s8084948.
15. Z. Zlatko Petrov, "Detection of targets in foliage clutter, based on multiresolutional denoising," in *Proc. Int. Conf. on Comput. as a Tool*, Vol. 2, pp. 1590–1593, IEEE, Belgrade, Serbia (2005).
16. Z. Du et al., "A new method for ship detection in SAR imagery based on combinatorial PNN model ," in *Proc. IEEE 1st Int. Conf. on Intelligent Networks and Intelligent Systems*, pp. 531–534, IEEE, Wuhan, China (2008).
17. X. W. Xing et al., "A fast algorithm based on two-stage CFAR for detecting ships in SAR images," in *Proc. IEEE 2nd Asian-Pacific Conf. on Synthetic Aperture Radar*, pp. 506–509, IEEE, Xian, Shanxi, China (2009).
18. J. Ai et al., "A new CFAR ship detection algorithm based on 2-D joint log-normal distribution in SAR images," *IEEE Trans. Geosci. Rem. Sens. Lett.* **7**(4), 806–810 (2010), http://dx.doi.org/10.1109/LGRS.2010.2048697.
19. M. Tello, C. Lopez-Martinez, and J. J. Mallorqui, "A novel algorithm for ship detection in SAR imagery based on the wavelet transform," *IEEE Trans. Geosci. Rem. Sens. Lett.* **2**(2), 201–205 (2005), http://dx.doi.org/10.1109/LGRS.2005.845033.
20. R. Marques, F. N. S. de Medeiros, and D. M. Ushizima, "Target detection in SAR images based on a level set approach," *IEEE Trans. Syst. Man Cybern. C* **39**(2), 214–222 (2009), http://dx.doi.org/10.1109/TSMCC.2008.2006685.
21. M. Liao et al., "Using SAR images to detect ships from sea clutter," *IEEE Geosci. Rem. Sens. Lett.* **5**(2), 194–198 (2008), http://dx.doi.org/10.1109/LGRS.2008.915593.
22. C. Zhuo, "An improved automatic ship detection method in SAR images," in *Proc. IEEE 2nd Int. Congress on Image and Signal Process.*, pp. 1–4, IEEE, Tianjin, China (2009).
23. M. Migliaccio, A. Gambardella, and F. Nunziata, "Ship detection over single-look complex SAR images," in *Proc. IEEE/OES US/EU-Baltic Int. Symposium*, pp. 1–4, IEEE, Tallinn, Estonia (2008).
24. S.-I. Hwang and K. Ouchi, "On a novel approach using MLCC and CFAR for the improvement of ship detection by synthetic aperture radar ," *IEEE Trans. Geosci. Rem. Sens. Lett.* **7**(2), 391–395 (2010), http://dx.doi.org/10.1109/LGRS.2009.2037341.
25. C. H. Jung et al., "Double-step fast CFAR scheme for multiple target detection in high resolution SAR images," in *Proc. IEEE Radar Conf.*, pp. 1172–1175, IEEE, Washington, DC (2010).
26. G. Gao, "A Parzen-Window-Kernel-based CFAR algorithm for ship detection in SAR images," *IEEE Geosci. Rem. Sens. Lett.* **8**(3), 557–561 (2011), http://dx.doi.org/10.1109/LGRS.2010.2090492.
27. M. Migliaccio et al., "A physically consistent speckle model for marine SLCSAR images," *IEEE J. Ocean. Eng.* **32**(4), 839–848 (2007), http://dx.doi.org/10.1109/JOE.2007.903985.
28. A. M. Treisman and G. Gelade, "A feature-integration theory of attention," *Cognit. Psychol.* **12**(1), 97–136 (1980), http://dx.doi.org/10.1016/0010-0285(80)90005-5.
29. C. Koch and S. Ullman, "Shifts in selective visual attention: towards the underlying neural circuitry," *Human Neurobiol.* **4**(4), 219–227 (1985).
30. L. Itti, C. Koch, and E. Niebur, "A model of saliency-based visual attention for rapid scene analysis," *IEEE Trans. Pattern Anal. Mach. Intell.* **20**(11), 1254–1259 (1998), http://dx.doi.org/10.1109/34.730558.

31. X. Hou and L. Zhang, "Saliency detection: a spectral residual approach," in *Proc. IEEE Conf. on Comput. Vis. and Pattern Recognit.*, pp. 1–8, IEEE , Minneapolis, Minnesota (2007).
32. C. Guo, Q. Ma, and L. Zhang, "Spatio-temporal Saliency detection using phase spectrum of quaternion Fourier transform ," in *Proc. IEEE Conf. on Comput. Vis. and Pattern Recognit.*, pp. 1–8, IEEE, Anchorage Alaska (2008).
33. P. Bian and L. Zhang, "Biological plausibility of spectral domain approach for spatiotemporal visual saliency," in *Proc. 15th Int. Conf. on Adv. in Neuro-Information Process.*, pp. 251–258, Springer-Verlag, Berlin, Heidelberg (2009).
34. Y. Yu, B. Wang, and L. Zhang, "Pulse discrete cosine transform for saliency-based visual attention," in *Porc. IEEE 8th Int. Conf. on Development and Learning*, pp. 1–6, IEEE, Shanghai, China (2009).
35. Y. Yu, B. Wang, and L. Zhang, "Hebbian-based neural networks for bottom-up visual attention systems," in *Proc. 16th Int. Conf. on Neural Inform. Process.: Part I* , pp. 1–6, Springer-Verlag, Berlin, Heidelberg (2009).
36. M. Tello, C. Lopez-Martinez, and J. Mallorqui, "A novel approach for the automatic detection of punctual isolated targets in a noisy background in SAR imagery," in *Proc. IEEE European Radar Conf.*, pp. 41–44, IEEE, Paris, France (2005).
37. N. Ahmed, T. Natarajan, and K. R. Rao, "Discrete cosine transform," *IEEE Trans. Comput.* **C-23**(1), 90–93 (1974), http://dx.doi.org/10.1109/T-C.1974.223784.
38. http://earth.esa.int/ers/ers_action/_corsica_details.html://earth.esa.int/ers/ers_action/_corsica_details.html.
39. http://www.neodaas.ac.uk/supportedscience/radardata.php (22 Jun. 2008).
40. T. Fawcett, "An introduction to ROC analysis," *Pattern Recogn. Lett.* **27**(8), 861–874 (2006), http://dx.doi.org/10.1016/j.patrec.2005.10.010.

Biographies and photographs of the authors are not available.